Multiscale calculations of thermoelectric properties of *n*-type $Mg_2Si_{1-x}Sn_x$ solid solutions

X. J. Tan,[1] W. Liu,[2] H. J. Liu,[1,*] J. Shi,[1] X. F. Tang,[2] and C. Uher[3]

[1]*Key Laboratory of Artificial Micro- and Nano-structures of Ministry of Education and School of Physics and Technology, Wuhan University, Wuhan 430072, China*

[2]*State Key Laboratory of Advanced Technology for Materials Synthesis and Processing, Wuhan University of Technology, Wuhan 430070, China*

[3]*Department of Physics, University of Michigan, Ann Arbor, Michigan, 48109, USA*

(Received 13 April 2012; published 31 May 2012)

The band structure of $Mg_2Si_{1-x}Sn_x$ solid solutions with $0.250 \leqslant x \leqslant 0.875$ is calculated using the first-principles pseudopotential method. It is found that the low-lying light and heavy conduction bands converge and the effective mass reaches a maximum value near $x = 0.625$. Using the semiclassical Boltzmann transport theory and relaxation-time approximation, we find that the system with $x = 0.625$ exhibits both higher Seebeck coefficient and higher electrical conductivity than other solid solutions at intermediate temperatures. By fitting first-principles total energy calculations, a modified Morse potential is constructed, which is used to predicate the lattice thermal conductivity via equilibrium molecular dynamics simulations. Due to relatively higher power factor and lower thermal conductivity, the $Mg_2Si_{0.375}Sn_{0.625}$ is found to exhibit enhanced thermoelectric performance at 800 K, and additional Sb doping is considered in order to make a better comparison with experiment results.

DOI: 10.1103/PhysRevB.85.205212 PACS number(s): 72.15.Jf, 71.15.Mb, 71.20.−b, 66.70.Df

I. INTRODUCTION

As fossil fuels are being exhausted and their burning contributes to the global warming, it is urgently needed to develop clean and renewable sources of energy. Thermoelectric materials have attracted much attention because they can directly convert heat into electricity and vice versa. Such materials utilize the Seebeck effect for power generation and the Peltier effect for refrigeration. The efficiency of a thermoelectric material is determined by the so-called figure of merit

$$ZT = S^2\sigma T/\kappa, \tag{1}$$

where S is the Seebeck coefficient, σ is the electrical conductivity, T is the absolute temperature, and κ is the thermal conductivity which contains both the lattice (κ_l) and electronic components (κ_e). A high ZT value indicates good thermoelectric performance, and one therefore should try to increase the power factor ($S^2\sigma$) and/or decrease the thermal conductivity ($\kappa = \kappa_e + \kappa_l$). [1]

Intermetallic compounds Mg_2Si, Mg_2Sn, and their solid solutions could be promising thermoelectric materials at intermediate temperature range between 500–800 K. These compounds contain nontoxic and environmentally friendly constituent elements that are inexpensive and abundant in the Earth's crust.[2,3] Mg_2Si can be readily *n*-type doped, and the usual donors are Bi and Sb. For example, Tani and Kido[4] fabricated the $Mg_2SiBi_{0.02}$ sample which exhibited a ZT value of 0.86 at 862 K. Akasaka *et al.*[5] obtained a ZT value of 0.65 at 840 K for the Mg_2Si:$Bi_{0.01}$. Bux *et al.*[6] found a ZT value of 0.7 at 775 K for the $Mg_2SiBi_{0.0015}$. You *et al.*[7] prepared the Mg_2Si:$Bi_{0.02}$ sample with a ZT value of 0.7 at 823 K. The Sb-doped sample $Mg_2SiSb_{0.02}$ has a ZT value of 0.56 at 862 K,[8] while the $Mg_2Si_{0.9}Sb_{0.1}$ shows a ZT value of 0.55 at 750 K.[9] On the other hand, Zaitsev *et al.*[10] investigated *n*-type $Mg_2Si_{1-x}Sn_x$ solid solutions in a broad range of compositions, and found that the large atomic mass difference between Si and Sn dramatically reduces the thermal conductivity of the solid solutions, which leads to a high-ZT value of about 1.1 near 800 K. Isoda *et al.*[11] obtained a ZT value of 0.87 at 630 K for the Bi-doped $Mg_2Si_{0.5}Sn_{0.5}$. Tani and Kido[12] found that the Al-doped $Mg_2Si_{0.9}Sn_{0.1}$ shows a ZT value of 0.68 at 864 K, which is six times larger than that of the undoped solid solution. Luo *et al.*[13] fabricated the $Mg_2Si_{1-x}Sn_x$ ($0 \leqslant x \leqslant 1.0$) solid solutions and enhanced the ZT value to 0.1 at 490 K when $x = 0.2$. Liu *et al.*[14] prepared the low-cost Sb-doped $Mg_2Si_{0.6}Sn_{0.4}$, and the ZT value can be reached to 1.11 at 860 K. Gao *et al.*[15] reproducibly obtained ZT values larger than 0.9 at 780 K for their Sb-doped $Mg_2Si_{0.5}Sn_{0.5}$. Based on the symmetry of energy bands of Mg_2Si and Mg_2Sn, Zaitsev *et al.*[10] reasoned that for some particular content of Si and Sn, the two low-lying conduction bands of $Mg_2Si_{1-x}Sn_x$ solid solutions will coincide in energy but did not consider consequences of such a band convergence. Very recently, the positive effect of band convergence on the Seebeck coefficient and thus the overall thermoelectric performance of $Mg_2Si_{1-x}Sn_x$ solid solutions was experimentally demonstrated by our team[16] and yielded a ZT value of 1.3 around 750 K.

The above survey indicates that the measured ZT value of Mg_2Si-based materials varies in the range of 0.1–1.3 and depends on the condition of synthesis, alloying proportions, and doping levels. However, the bulk of these works were focused on experimental studies with little theoretical insight and guidance provided. In this work, we investigate the thermoelectric properties of *n*-type doped $Mg_2Si_{1-x}Sn_x$ ($0.250 \leqslant x \leqslant 0.875$) solid solutions by a multiscale approach, which includes first-principles calculations, semiclassical Boltzmann transport theory, and empirical molecular dynamics (MD) simulations. We shall see that the $Mg_2Si_{1-x}Sn_x$ with $x = 0.625$ exhibits the highest ZT value at 800 K due to the highest power factor and the lowest thermal conductivity, which suggests its promising thermoelectric applications.

The rest of this paper is organized as follows. Sec. II gives the computational details of our multiscale approach.

In Sec. III, we discuss the electronic, transport, and thermoelectric properties of n-type $Mg_2Si_{1-x}Sn_x$ ($0.250 \leqslant x \leqslant 0.875$) solid solutions. A summary of our work is given in Sec. IV.

II. METHOD OF CALCULATIONS

A. First-principles calculations and Boltzmann theory

The energy band-structure calculations have been performed using a first-principles plane-wave pseudopotential formulation[17–19] within the framework of density functional theory (DFT). The exchange-correlation energy is in the form of Perdew-Wang-91 (Ref. 20) with generalized gradient approximation (GGA). Ultrasoft pseudopotentials are used for the Mg, Si, and Sn atoms and the cutoff energy is set as 151 eV. During the geometry optimizations, both the atomic positions and the lattice constants are fully relaxed until the magnitude of the force acting on all atoms becomes less than 0.01 eV/Å, which also converges the total energy within 1 meV. The irreducible Brillouin zone (IBZ) is sampled with $10 \times 10 \times 10$ Monkhorst-Pack $\boldsymbol{k}$ meshes. The $Mg_2Si_{1-x}Sn_x$ solid solutions are modeled by a rhombohedral $2 \times 2 \times 2$ supercell which has eight equivalent positions for the Si or Sn atoms. The Sn concentration x can thus be 0.250, 0.375, 0.500, 0.625, 0.750, and 0.875, which are comparable to those measured in Ref. 16.

In a microscopic model of transport process, the Seebeck coefficient S, the electrical conductivity σ, and the electronic thermal conductivity κ_e can be derived from the calculated band structure in the IBZ. Here, we use a semiclassical approach by solving the Boltzmann's equation in the relaxation-time approximation.[21] The kernel is to find the so-called transport distribution, which can be expressed as

$$\Xi = \sum_{\vec{k}} \vec{v}_{\vec{k}} \vec{v}_{\vec{k}} \tau_{\vec{k}}, \tag{2}$$

where $\vec{v}_{\vec{k}}$ and $\tau_{\vec{k}}$ are the group velocity and relaxation time at state $\vec{k}$, respectively. In principle, the relaxation time is energy dependent. However, it is usually reasonable to assume a constant τ for transport properties since they involve the derivative of the Fermi function, which is significant only in a small energy window around the Fermi level and τ usually does not change much over this interval.[22] The Seebeck coefficient S and the electrical conductivity σ are given by

$$\sigma = e^2 \int d\varepsilon \left(-\frac{\partial f_0}{\partial \varepsilon}\right) \Xi(\varepsilon), \tag{3}$$

$$S = \frac{e k_B}{\sigma} \int d\varepsilon \left(-\frac{\partial f_0}{\partial \varepsilon}\right) \Xi(\varepsilon) \frac{\varepsilon - \mu}{k_B T}, \tag{4}$$

where f_0 is the equilibrium Fermi function, k_B is the Boltzmann's constant, and μ is the chemical potential. The electronic thermal conductivity κ_e is calculated according to the Wiedemann-Franz law[23]

$$\kappa_e = L \sigma T, \tag{5}$$

where L is the Lorenz number.

B. Empirical potential and molecular dynamics

To study the phonon transport in the $Mg_2Si_{1-x}Sn_x$ solid solutions, an accurate interatomic potential is necessary. We thus develop a modified Morse potential which contains the two-body bond and three-body angle interactions

$$U = U_1 + U_2. \tag{6}$$

Here, the two-body potential U_1 is in the form of[24]

$$U_1 = D\{[1 - e^{-a(r-r_0)}]^2 - 1\}, \tag{7}$$

where D is the depth of the potential well, a is the bond elasticity, r represents the interatomic separation, and r_0 is the corresponding equilibrium distance. The three-body potential U_2 is given by[24]

$$U_2 = \tfrac{1}{2} k (\cos\theta - \cos\theta_0)^2, \tag{8}$$

where k is the force constant, θ represents the bond angle, and θ_0 is the corresponding angle at equilibrium. These potential parameters can be determined by fitting the energy surface from first-principles calculations.

The lattice thermal conductivity κ_l is then predicted using MD simulations combined with the Green-Kubo autocorrelation decay method.[24,25] Such an approach can deal with phonon-phonon scattering and it is possible to obtain an accurate κ_l from the periodic unit cell much smaller than the phonon mean-free path. In this work, the time step is set as 0.5 fs, and the constant temperature simulation with periodic boundary conditions runs for 4 000 000 steps, giving a total time of 2.0 ns. The system reaches an equilibrium state and the temperature stabilizes around the set value after 0.5 ns. The data collection is performed from 0.5 to 2.0 ns and the

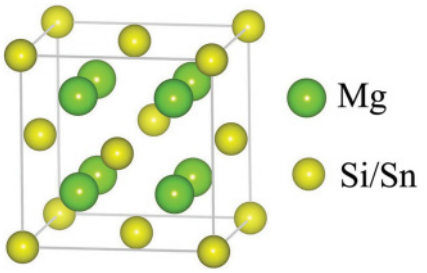

FIG. 1. (Color online) The crystal structure of antifluorite compounds Mg_2Si and Mg_2Sn.

TABLE I. Calculated lattice constant a (in unit of Å), effective mass m^*(in terms of electron mass m_0), and the energy difference ΔE (in units of eV) between the two low-lying conduction bands (CB_L and CB_H) for the $Mg_2Si_{1-x}Sn_x$ solid solutions.

		m^*		
x	a	CB_L	CB_H	ΔE
0.000	6.35			
0.250	6.46	0.19	0.38	0.30
0.375	6.52	0.24	0.43	0.18
0.500	6.59	0.26	0.43	0.11
0.625	6.64	0.20	0.61	0.038
0.750	6.70	0.25	0.52	0.15
0.875	6.76	0.28	0.37	0.27
1.000	6.81			

corresponding heat flux J is given by

$$J = \sum_i \varepsilon_i v_i + \frac{1}{2}\sum_{i<j}[f_{ij}\cdot(v_i + v_j)]r_{ij}, \quad (9)$$

where ε_i is the site energy of atom i, $v_i$and v_j are, respectively, the velocities of atoms i and j, f_{ij} is their interaction force, and r_{ij} is their separation. The lattice thermal conductivity κ_l is thus obtained by

$$\kappa_l = \frac{1}{3k_B T^2 V}\int_0^\infty \langle J(0)\cdot J(t)\rangle dt, \quad (10)$$

where V is the volume of the simulation system, and $\langle J(0)\cdot J(t)\rangle$ is the so-called heat-flux autocorrelation function. Our results are carefully tested with respect to the total MD simulation time and the size of the simulation box.

III. RESULTS AND DISCUSSIONS

We begin our discussions with the crystal structures of Mg_2Si/Mg_2Sn shown in Fig. 1. Pristine Mg_2Si (Mg_2Sn) has a face-centered-cubic antifluorite lattice with $Fm\bar{3}m$ space group. The unit cell contains four primitive cells with the Mg and Si (Sn) atoms located at the 8c: (0.25, 0.25, 0.25) and 4a: (0, 0, 0) sites, respectively. The calculated lattice constants are $a = 6.35$ and 6.81 Å for the Mg_2Si and Mg_2Sn, respectively. These values are very close to those found experimentally.[26] The optimized lattice constants of a series of $Mg_2Si_{1-x}Sn_x$ ($0.250 \leqslant x \leqslant 0.875$) solid solutions are summarized in Table I, which increases almost linearly from 6.47 to 6.76 Å as the Sn concentration x is increased.[13,27] In particular, the calculated lattice constant ($a = 6.59$ Å) for the $Mg_2Si_{0.5}Sn_{0.5}$ agrees well with the measured value ($a = 6.56$ Å),[13] which confirms the reliability of our theoretical calculations.

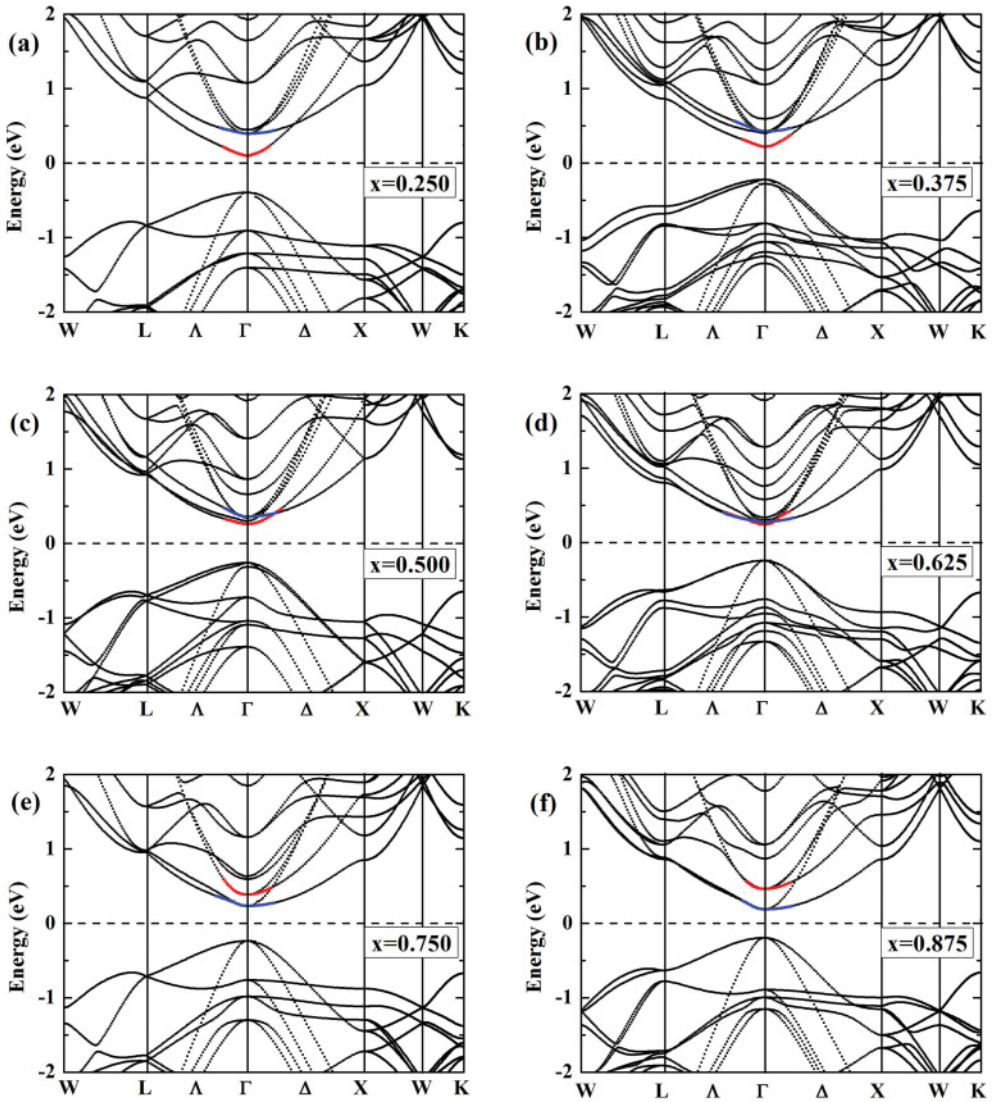

FIG. 2. (Color online) Calculated energy band structures for a series of $Mg_2Si_{1-x}Sn_x$ solid solutions. The red and blue lines correspond to the light and heavy conduction bands, respectively. The Fermi level is at 0 eV.

A. Energy band structure

Figures 2(a)–2(f) show the calculated energy band structures for a series of $Mg_2Si_{1-x}Sn_x$ solid solutions. As known, both Mg_2Si and Mg_2Sn are indirect gap semiconductors. The valence-band maximum (VBM) is located at the Γ point, while the conduction-band minimum (CBM) at the X point. However, we see from Fig. 2 that all the $Mg_2Si_{1-x}Sn_x$ solid solutions become direct gap semiconductors where both the VBM and the CBM appear at the Γ point. This is due to the fact that we are using a $2 \times 2 \times 2$ supercell rather than the primitive cell and the bands are thus folded. It should be noted that DFT tends to underestimate the energy gap, therefore, all the calculated band gaps of the $Mg_2Si_{1-x}Sn_x$ solid solutions are corrected in this work. We find that the difference between experimental[26] and calculated gap is almost the same for the Mg_2Si and Mg_2Sn. For simplicity, we thus make a uniform shift of the calculated band gaps for all the solid solutions. If we focus on the two low-lying conduction bands around the Γ point, we see that with the Sn content x increasing from 0.250 to 0.875, the heavy conduction band (CB_H, blue) shifts down while the light conduction band (CB_L, red) shifts up. As a result, these two bands converge at $x = 0.625$. We have calculated the band-decomposed charge-density contour (not shown here), and find that the lowest conduction band has Si character for the Mg_2Si, while Sn character for the Mg_2Sn. In the case of the $Mg_2Si_{1-x}Sn_x$, the lowest conduction band exhibits both Si and Sn character; however, the major contribution comes from Si when $0.25 \leqslant x < 0.625$, and from Sn when $0.625 < x \leqslant 0.875$. This is consistent with the fact that the lowest conduction band of $Mg_2Si_{1-x}Sn_x$ is the light band for $0.25 \leqslant x < 0.625$ but is the heavy band for $0.625 < x \leqslant 0.875$ (see Fig. 2). At $x = 0.625$, the light and heavy bands converge and the charge-density contour indicates that the contributions from Si and Sn are nearly equal to each other. Overall speaking, the effective mass of the lowest conduction band increases with the Sn content x, reaches a maximum at $x = 0.625$, and then decreases. Both the convergence of the conduction bands and the increased effective mass lead to a high absolute value of the Seebeck coefficient,[1,28] which is very beneficial to the thermoelectric performance. We will come back to this point later. The energy difference between the CB_H and CB_L as well as their effective masses are summarized in Table I.

B. Relaxation time and electrical conductivity

Based on the calculated band structures, we are able to evaluate the electronic transport coefficients of the $Mg_2Si_{1-x}Sn_x$ solid solutions by using the semiclassical Boltzmann theory and the rigid-band approach.[29] To get reliable results, we use a very dense $\boldsymbol{k}$ mesh up to 1000 points in our calculations. It should be mentioned that the electrical conductivity σ can only be calculated with respect to the electron relaxation time τ, that is, what we actually get is σ/τ. The relaxation time is then determined by comparing the experimentally measured electrical conductivity σ (Ref. 16) at a particular carrier concentration and temperature. The fitted relaxation time for the solid solutions is summarized in Table II. We see

TABLE II. Determining the electron relaxation time τ for the $Mg_2Si_{1-x}Sn_x$ solid solutions by comparing the experimentally measured electrical conductivity at different carrier concentration and temperature.

		τ (fs)					
x	n (10^{20} cm^{-3})	300 K	400 K	500 K	600 K	700 K	800 K
0.25	1.70	11.4	9.28	7.87	6.26	5.22	4.31
	2.10	12.3	10.1	8.13	6.85	5.7	4.43
	(Mean value)	11.8	9.7	8.0	6.6	5.5	4.4
0.375	1.35	6.74	5.54	4.85	4.17	3.54	2.95
	1.80	6.32	5.27	4.31	3.76	3.23	2.74
	2.35	6.44	5.41	4.46	3.62	3.10	2.59
	(Mean value)	6.5	5.4	4.5	3.8	3.3	2.8
0.5	1.90	5.43	4.62	3.84	3.39	2.74	2.37
	2.39	3.99	3.4	2.86	2.57	2.15	1.96
	2.84	4.41	3.82	3.26	2.74	2.28	1.99
	(Mean value)	4.6	3.9	3.3	2.9	2.4	2.1
0.625	0.63	7.65	6.71	5.58	4.55	4.09	3.73
	1.68	6.97	5.80	4.75	4.18	3.59	2.98
	(Mean value)	7.3	6.3	5.1	4.4	3.8	3.4
0.75	1.57	6.34	5.09	4.06	3.51	2.83	2.61
	1.69	6.99	5.67	4.56	3.93	3.39	2.92
	1.72	6.78	5.96	4.79	3.83	3.30	2.84
	2.13	6.95	5.58	4.45	3.86	3.13	1.69
	(Mean value)	6.8	5.6	4.5	3.8	3.2	2.5
0.875	1.70	7.87	6.44	5.14	4.06	3.41	2.87
	2.30	8.21	6.69	5.52	4.58	3.73	2.99
	(Mean value)	8.0	6.6	5.3	4.3	3.6	2.9

that the relaxation time does not vary much in the carrier-concentration range considered. In contrast, there is obvious temperature dependence. As a reasonable approximation, in the following discussions we use an average relaxation time at each temperature. For a particular x, we see from Table II that the relaxation time decreases with increasing temperature. This is reasonable since the electron scattering is more frequent at high temperatures. At a particular temperature, we see that the relaxation time decreases before reaching a minimum value at $x = 0.5$ and then increases, suggesting that the solid solution at $x = 0.5$ is of highest disorder as far as the carrier transport is concerned.

Figure 3(a) plots the calculated electrical conductivity σ as a function of temperature for the $Mg_2Si_{1-x}Sn_x$ solid solutions, where the doping level (or carrier concentration) of each system is fixed at 1.9×10^{20} cm^{-3}. In the temperature range of 300–800 K, we see that the electrical conductivity decreases with increasing temperature. This is believed to be caused by the reduced electron mobility at high temperatures, while the carrier (electron) concentration remains almost constant with temperature. It is interesting that the calculated σ of $Mg_2Si_{0.375}Sn_{0.625}$ decreases relatively slower with increasing temperature and is higher than those of the other solid solutions except $x = 0.250$ and 0.875 at intermediate temperatures. On the other hand, we plot in Fig. 3(b) the calculated electrical conductivity σ as a function of carrier concentration, where the temperature is fixed at 800 K. As expected, the electrical conductivity σ increases with increasing carrier concentration n. The electrical conductivity of $Mg_2Si_{0.750}Sn_{0.250}$ and $Mg_2Si_{0.375}Sn_{0.625}$ are higher than those of the other solid solutions with $Mg_2Si_{0.625}Sn_{0.375}$ and $Mg_2Si_{0.500}Sn_{0.500}$ exhibiting the lowest values.

C. Seebeck coefficient and power factor

Figure 4(a) shows the calculated Seebeck coefficient S as a function of temperature for the $Mg_2Si_{1-x}Sn_x$ solid solutions at a carrier concentration of 1.9×10^{20} cm^{-3}. It is found that the absolute value of the Seebeck coefficient increases with increasing temperature. Compared with the experimentally measured result of $Mg_2Si_{0.500}Sn_{0.500}$, the calculated S exhibits a similar variation with temperature, but the absolute value is somehow underestimated. In Fig. 4(b), we plot the calculated Seebeck coefficient at 800 K as a function of carrier concentration in the range of 10^{19}–10^{21} cm^{-3}. We see the absolute value of Seebeck coefficient increases initially, reaches a maximum, and then decreases as the carrier concentration increases. As mentioned above, when the two conduction bands converge and the effective mass increases, one can obtain a very large absolute value of Seebeck coefficient. Indeed, except at very low carrier concentrations, $Mg_2Si_{0.375}Sn_{0.625}$ exhibits the highest absolute value of S among these solid solutions.

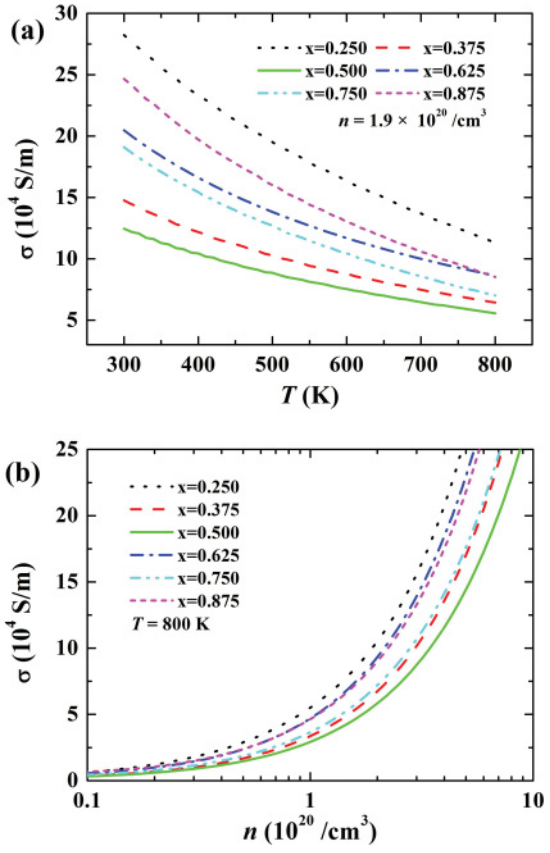

FIG. 3. (Color online) (a) Calculated electrical conductivity σ of $Mg_2Si_{1-x}Sn_x$ solid solutions as a function of temperature. All systems have a carrier concentration of 1.9×10^{20} cm^{-3}. (b) Calculated σ as a function of carrier concentration n (10^{19}–10^{21} cm^{-3}) at 800 K.

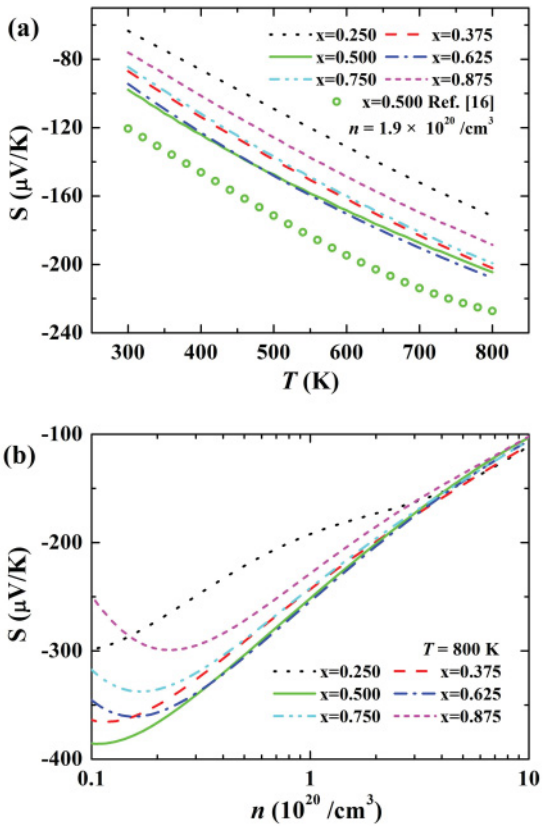

FIG. 4. (Color online) (a) Calculated Seebeck coefficient S of $Mg_2Si_{1-x}Sn_x$ solid solutions as a function of temperature. All systems have a carrier concentration of 1.9×10^{20} cm^{-3}, and the measured result of $Mg_2Si_{0.500}Sn_{0.500}$ is also shown. (b) Calculated S as a function of carrier concentration n (10^{19}–10^{21} cm^{-3}) at 800 K.

Although there is some underestimation of the calculated Seebeck coefficient, it is still more than 250 μV/K for the $Mg_2Si_{0.375}Sn_{0.625}$ at a carrier concentration of 10^{20} cm^{-3}, which is close to those measured previously.[10,14,30] We want to mention that the underestimation of the calculated Seebeck coefficient indicated in Fig. 4(a) can be attributed to the fact that in the experiment,[16] the sample prepared deviates a little from the standard nominal formula of $Mg_2Si_{0.5}Sn_{0.5}$ and has a real composition of $Mg_{2.11}Si_{0.52}Sn_{0.48}Sb_{0.006}$. Here, the Mg excess was found to increase the absolute value of the Seebeck coefficient.[33]

Figure 5(a) shows the calculated power factor $S^2\sigma$ as a function of temperature for the $Mg_2Si_{1-x}Sn_x$ solid solutions at a carrier concentration of 1.9×10^{20} cm^{-3}. As discussed above, the $Mg_2Si_{0.375}Sn_{0.625}$ exhibits the highest absolute value of Seebeck coefficient S due to the band convergence and enhanced effective mass. It also has a relatively higher electrical conductivity σ, especially at intermediate temperatures. Consequently, the power factor of $Mg_2Si_{0.375}Sn_{0.625}$ is much higher than those of the other solid solutions in the whole temperature range from 300 to 800 K. On the other hand, we plot in Fig. 5(b) the power factor at 800 K as a function of carrier concentration in the range of 10^{19}–10^{21} cm^{-3}. As known, the Seebeck coefficient decreases with increasing carrier concentration, while the electrical conductivity increases. In a broad range of carrier concentrations, the power factor should therefore increase initially, reach a maximum value, and then decrease. Within the carrier concentration considered in this work, we see from Fig. 5(b) that the power factor increases monotonously. The calculated value of $Mg_2Si_{0.375}Sn_{0.625}$ at 800 K is about 3.1×10^{-3} W/mK^2 with a carrier concentration of 10^{20} cm^{-3}, which is somehow higher than that of other Mg_2Si-based thermoelectric materials.[15,31,32]

D. Electronic thermal conductivity

We now discuss the electronic thermal conductivity κ_e of the $Mg_2Si_{1-x}Sn_x$ solid solutions. As mentioned before, the κ_e can be derived from σ using Eq. (5). Here, the Lorenz number L for the $Mg_2Si_{1-x}Sn_x$ solid solutions is estimated based on the Fermi-Dirac statistics noted in Ref. 11 which attains the fully degenerate value of 2.45×10^{-8} V^2/K^2 as the carrier concentration reaches typical metallic densities. For the $Mg_2Si_{1-x}Sn_x$ solid solutions, the Lorenz number is found to be $1.8 \sim 1.9 \times 10^{-8}$ V^2/K^2 around the carrier concentration of 10^{20} cm^{-3} (Refs. 11 and 33) and is therefore used in our calculations. Figure 6(a) shows the temperature dependence of the calculated κ_e for the $Mg_2Si_{1-x}Sn_x$ series at a carrier concentration of 1.9×10^{20} cm^{-3}. The general trend observed is an initial mild increase followed by a rather undistinguished maximum and finally a slowly decreasing conductivity. The

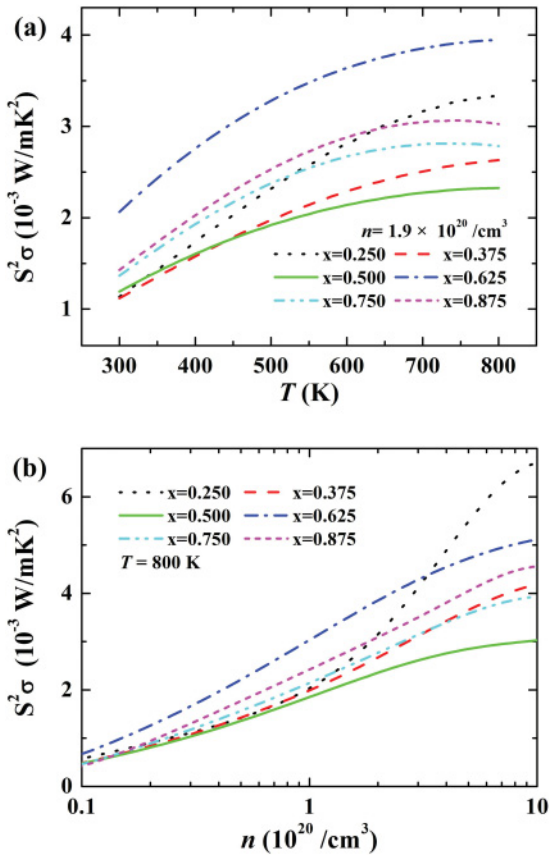

FIG. 5. (Color online) (a) Calculated power factor $S^2\sigma$ of $Mg_2Si_{1-x}Sn_x$ solid solutions as a function of temperature. All systems have a carrier concentration of 1.9×10^{20} cm^{-3}. (b) Calculated $S^2\sigma$ as a function of carrier concentration n (10^{19}–10^{21} cm^{-3}) at 800 K.

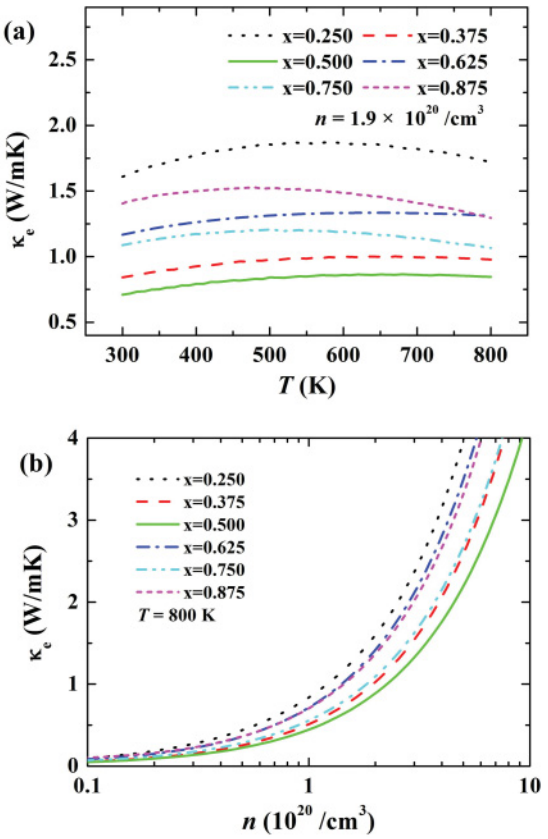

FIG. 6. (Color online) (a) Calculated electronic thermal conductivity κ_e of $Mg_2Si_{1-x}Sn_x$ solid solutions as a function of temperature. All systems have a carrier concentration of 1.9×10^{20} cm^{-3}. (b) Calculated κ_e as a function of carrier concentration n (10^{19}–10^{21} cm^{-3}) at 800 K.

calculated κ_e of $Mg_2Si_{0.375}Sn_{0.625}$ is 1.17 W/mK at 300 K and 1.31 W/mK at 800 K.

As shown in Fig. 6(b), the carrier-concentration dependence of the electronic thermal conductivity κ_e at 800 K mimics the behavior of the electrical conductivity σ, i.e., it increases monotonously with increasing carrier concentration. The $Mg_2Si_{0.750}Sn_{0.250}$ and $Mg_2Si_{0.375}Sn_{0.625}$ solid solutions exhibit higher κ_e than the others in the whole carrier-concentration range from 10^{19} to 10^{21} cm^{-3}. Compared with the power factor shown in Fig. 5(b), the electronic thermal conductivity of $Mg_2Si_{0.375}Sn_{0.625}$ decreases faster with decreasing carrier concentration n around 10^{20} cm^{-3}. For example, as n decreases from 2.0 to 1.0 $\times$ 10^{20} cm^{-3} at 800 K, the κ_e of $Mg_2Si_{0.375}Sn_{0.625}$ falls by 48%, while the power factor $S^2\sigma$ is reduced by only 21%. In the following discussions, we shall see that such a trend is important for optimizing the thermoelectric performance of these solid solutions.

E. Lattice thermal conductivity

To deal with the phonon transport, we have performed MD simulations where a modified Morse potential is constructed

TABLE III. Fitted parameters in the modified Morse potential for the Mg_2Si, Mg_2Sn, and $Mg_2Si_{1-x}Sn_x$ solid solutions.

		Two-body			Three-body		
		D (eV)	a (Å^{-1})	r_0 (Å)		k (eV)	θ_0 (°)
Mg_2Si	Mg-Mg	0.789	0.853	3.17	Si-Mg-Si	1.223	109.47
	Mg-Si	0.628	0.399	2.75	Mg-Si-Mg	1.120	109.47
	Si-Si	0.460	0.991	4.49	Mg-Si-Mg	1.120	70.53
$x = 0.250$	Mg-Mg	0.765	0.952	3.232	Si/Sn-Mg-Si/Sn	0.958	109.47
	Mg-Si	0.548	0.689	2.799	Mg-Si/Sn-Mg	0.958	109.47
	Mg-Sn	0.545	0.686	2.799	Mg-Si/Sn-Mg	0.942	70.53
	Si-Si	0.437	0.836	4.571			
	Sn-Sn	0.436	0.837	4.571			
	Si-Sn	0.434	0.835	4.571			
$x = 0.375$	Mg-Mg	0.898	0.924	3.257	Si/Sn-Mg-Si/Sn	1.106	109.47
	Mg-Si	0.639	0.576	2.821	Mg-Si/Sn-Mg	1.106	109.47
	Mg-Sn	0.635	0.574	2.821	Mg-Si/Sn-Mg	1.102	70.53
	Si-Si	0.481	0.873	4.606			
	Sn-Sn	0.481	0.872	4.606			
	Si-Sn	0.480	0.872	4.606			
$x = 0.500$	Mg-Mg	0.810	0.904	3.284	Si/Sn-Mg-Si/Sn	1.168	109.47
	Mg-Si	0.559	0.561	2.844	Mg-Si/Sn-Mg	1.168	109.47
	Mg-Sn	0.555	0.560	2.844	Mg-Si/Sn-Mg	1.164	70.53
	Si-Si	0.467	0.862	4.644			
	Sn-Sn	0.469	0.861	4.644			
	Si-Sn	0.468	0.858	4.644			
$x = 0.625$	Mg-Mg	0.735	0.789	3.316	Si/Sn-Mg-Si/Sn	1.144	109.47
	Mg-Si	0.569	0.536	2.872	Mg-Si/Sn-Mg	1.144	109.47
	Mg-Sn	0.568	0.538	2.872	Mg-Si/Sn-Mg	1.140	70.53
	Si-Si	0.461	0.862	4.489			
	Sn-Sn	0.462	0.859	4.489			
	Si-Sn	0.460	0.858	4.489			
$x = 0.750$	Mg-Mg	0.658	0.866	3.350	Si/Sn-Mg-Si/Sn	1.236	109.47
	Mg-Si	0.490	0.723	2.901	Mg-Si/Sn-Mg	1.236	109.47
	Mg-Sn	0.489	0.723	2.901	Mg-Si/Sn-Mg	1.228	70.53
	Si-Si	0.431	0.862	4.738			
	Sn-Sn	0.430	0.861	4.738			
	Si-Sn	0.428	0.863	4.738			
$x = 0.875$	Mg-Mg	0.883	0.894	3.380	Si/Sn-Mg-Si/Sn	1.328	109.47
	Mg-Si	0.681	0.455	2.927	Mg-Si/Sn-Mg	1.328	109.47
	Mg-Sn	0.682	0.452	2.927	Mg-Si/Sn-Mg	1.324	70.53
	Si-Si	0.453	0.658	4.780			
	Sn-Sn	0.454	0.661	4.780			
	Si-Sn	0.453	0.660	4.780			
Mg_2Sn	Mg-Mg	0.742	0.797	3.41	Sn-Mg-Sn	1.158	109.47
	Mg-Sn	0.597	0.356	2.95	Mg-Sn-Mg	1.140	109.47
	Sn-Sn	0.329	1.050	4.82	Mg-Sn-Mg	1.140	70.53

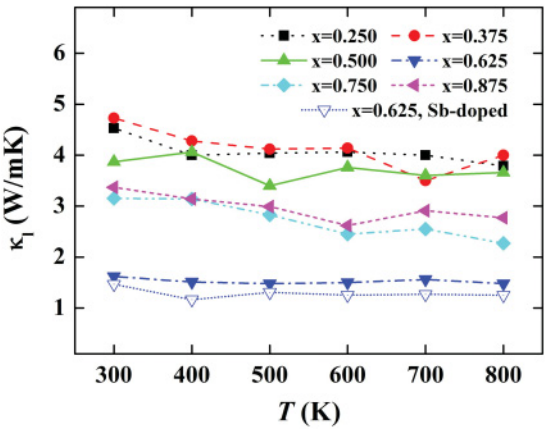

FIG. 7. (Color online) Calculated lattice thermal conductivity κ_l of $Mg_2Si_{1-x}Sn_x$ and Sb-doped $Mg_2Si_{0.375}Sn_{0.625}$ solid solutions at a temperature range from 300 to 800 K.

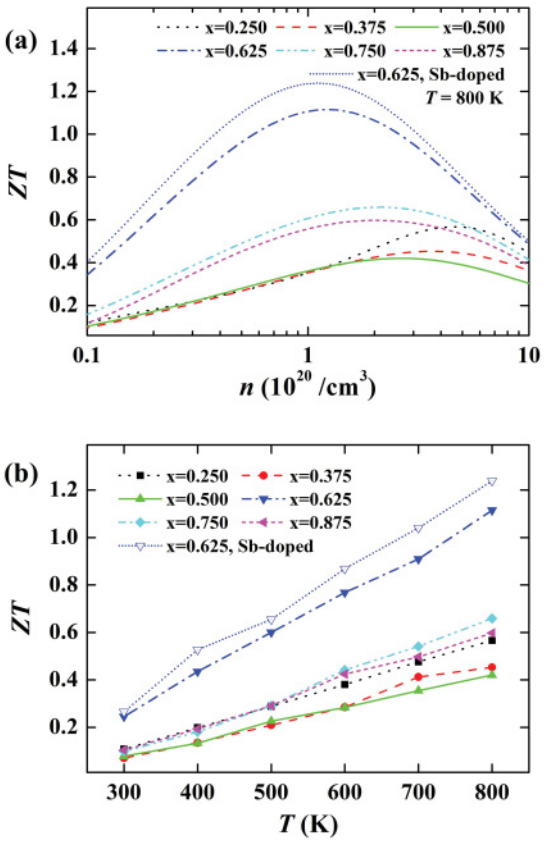

FIG. 8. (Color online) (a) Calculated ZT value of $Mg_2Si_{1-x}Sn_x$ and Sb-doped $Mg_2Si_{0.375}Sn_{0.625}$ solid solutions as a function of carrier concentration n (10^{19}–10^{21} cm^{-3}) at 800 K. (b) Calculated ZT value at optimal carrier concentration of $Mg_2Si_{1-x}Sn_x$ and Sb-doped $Mg_2Si_{0.375}Sn_{0.625}$ as a function of temperature.

by fitting the energy surface from first-principles calculations. Table III lists all the fitted potential parameters used in this work. Our calculated lattice thermal conductivity κ_l of Mg_2Si and Mg_2Sn is found to be 5.98 and 4.90 W/mK at 300 K, respectively. These values are consistent with those measured experimentally[13,26] and thus confirm the reliability of our MD simulations. The calculated κ_l for the $Mg_2Si_{1-x}Sn_x$ series is plotted in Fig. 7 in a wide temperature range. We see that the lattice thermal conductivity does not show strong temperature dependence. At any given temperature, the thermal conductivity initially decreases with increasing content of Sn. It reaches a clear minimum at $x = 0.625$ and then increases. Note that the minimum lattice thermal conductivity is obtained at $x = 0.625$ rather than at $x = 0.5$ where the Si and Sn should be most disordered. The calculated κ_l for $Mg_2Si_{0.375}Sn_{0.625}$ is only 1.62 W/mK at 300 K, representing merely 27% of that of the pure Mg_2Si. Such significant reduction in the lattice thermal conductivity is primarily a result of the large atomic mass difference between the Sn and Si that gives rise to a strong mass defect scattering. Our calculated variation of the lattice thermal conductivity as a function of Sn content is similar to the previously reported results. [13,16,26]

F. Optimized ZT value

With all transport coefficients available, we can now evaluate ZT values of the $Mg_2Si_{1-x}Sn_x$ solid solutions according to Eq. (1). Figure 8(a) shows the carrier-concentration dependence of the calculated ZT values at 800 K. As noted before, good thermoelectric performance requires a power factor $S^2\sigma$ as high as possible and a thermal conductivity $\kappa (= \kappa_e + \kappa_l)$ as low as possible. With higher $S^2\sigma$ and lower κ than the other solid solutions, we see that $Mg_2Si_{0.375}Sn_{0.625}$ exhibits superior thermoelectric performance in the whole carrier-concentration range ($n = 10^{19}$–10^{21} cm^{-3}). In particular, a ZT value of 1.11 can be achieved at 800 K with a carrier concentration of 1.2×10^{20} cm^{-3}. This is consistent with the conjecture that band convergence and the maximum effective mass will lead to enhanced thermoelectric performance. The ZT values of other $Mg_2Si_{1-x}Sn_x$ solid solutions, together with the optimal carrier concentration n, the power factor $S^2\sigma$, and the electronic and lattice thermal conductivities κ_e and κ_l are listed in Table IV.

Figure 8(b) plots the ZT values of these solid solutions as a function of temperature at optimal carrier concentrations. We see that the ZT values increase from 300 to 800 K, which is consistent with those found previously.[12,14–16] Moreover, all the $Mg_2Si_{1-x}Sn_x$ solid solutions exhibit higher ZT values at 800 K than at lower temperatures, which indicates that they could be applied as thermoelectric materials at intermediate temperatures. The optimized ZT value of 1.11 achieved at 800 K with $Mg_2Si_{0.375}Sn_{0.625}$ is by far the highest value among all the solid solutions.

Although a ZT value of 1.11 at 800 K is close to the maximum experimental value reported,[10,14,16,33] this is a very conservative value and we believe the thermoelectric performance of n-type $Mg_2Si_{1-x}Sn_x$ solid solutions could be further enhanced. It should be mentioned that up to now, we were considering electron and phonon transport in pristine $Mg_2Si_{1-x}Sn_x$ solid solutions. In real experiments, however, the different carrier concentrations are actually realized by doping these systems with Bi or Sb. According to previous experimental works,[9,16,30,32] appropriate doping not only enhances

TABLE IV. Optimized ZT values of $Mg_2Si_{1-x}Sn_x$ as well as Sb-doped $Mg_2Si_{0.375}Sn_{0.625}$ solid solutions at 800 K. The corresponding optimal carrier concentration n, the power factor $S^2\sigma$, and the electronic and lattice thermal conductivity κ_e and κ_l are also indicated.

x	n (10^{20} cm^{-3})	$S^2\sigma$ (10^{-3} W/mK^2)	κ_e (W/mK)	κ_l (W/mK)	ZT
0.250	4.5	5.20	3.54	3.79	0.57
0.375	3.6	3.32	1.86	4.00	0.45
0.500	2.7	2.54	1.18	3.66	0.42
0.625	1.2	3.24	0.85	1.48	1.11
0.625 (Sb-doped)	1.1	3.15	0.78	1.25	1.24
0.750	2.1	2.83	1.16	2.27	0.66
0.875	2.0	3.10	1.38	2.77	0.60

the power factor $S^2\sigma$, but can also significantly reduce the lattice thermal conductivity κ_l of Mg_2Si-based thermoelectric materials. To make a better comparison between our theoretical predications and the experimental results, we have done additional calculations where the lattice thermal conductivity κ_l of properly Sb-doped $Mg_2Si_{0.375}Sn_{0.625}$ is explicitly calculated. Indeed, it is found that κ_l is decreased by about 15% (see Fig. 7). As a result, the optimal carrier concentration is shifted to a value somewhat smaller than 1.1×10^{20} cm^{-3} as indicated in Fig. 8(a). At such carrier concentration, the power factor $S^2\sigma$ is slightly reduced from 3.24 to 3.15×10^{-3} W/mK^2. However, there is a faster decrease of the corresponding electronic thermal conductivity κ_e (from 0.85 to 0.78 W/mK), leading to a higher ZT value of 1.24 as indicated in both Fig. 8(a) and Table IV. We want to emphasize that the lattice thermal conductivity κ_l of the $Mg_2Si_{1-x}Sn_x$ solid solutions could be further reduced by many other means such as isotope doping[34] and embedded nanoinclusions,[35–37] which leave the power factor $S^2\sigma$ less affected. If the lattice thermal conductivity could be reduced to ~0.8 W/mK,[16] the optimized ZT values of $Mg_2Si_{0.375}Sn_{0.625}$ should reach 1.61 at 800 K, which would be very competitive, especially given the low cost and minimal environmental impact of this material system.

IV. SUMMARY

In summary, we have studied the thermoelectric properties of $Mg_2Si_{1-x}Sn_x$ ($0.250 \leqslant x \leqslant 0.875$) solid solutions using a multiscale approach. The convergence of the two conduction bands and the increased electron effective mass lead to a high value of the Seebeck coefficient for $x = 0.625$, which has been confirmed by explicit calculations of the electronic transport coefficients. On the other hand, $Mg_2Si_{0.375}Sn_{0.625}$ exhibits the lowest lattice thermal conductivity among all the solid solutions considered due to the high alloy disorder and a large Sn/Si mass difference scattering. Our theoretical results indicate that the maximum ZT value of $Mg_2Si_{1-x}Sn_x$ solid solutions is ~1.24 at 800 K for $x = 0.625$ with a carrier concentration of $n = 1.1 \times 10^{20}$ cm^{-3}. Moreover, we find that the ZT value is limited by the high lattice thermal conductivity, which for some solid solutions is as high as 4.0 W/mK. Therefore, there is still room to improve the thermoelectric performance of the $Mg_2Si_{1-x}Sn_x$ solid solutions. In any case, the n-type $Mg_2Si_{0.375}Sn_{0.625}$ is a very promising thermoelectric material, and major effort should be directed to developing comparatively effective p-type $Mg_2Si_{1-x}Sn_x$ solid solutions so that efficient thermoelectric modules based on this inexpensive and environmentally friendly material system could be realized.

ACKNOWLEDGMENTS

This work was supported by the "973 Program" of China (Grant No. 2007CB607501), the National Natural Science Foundation (Grant No. 51172167), and the Program for New Century Excellent Talents in University. C. Uher is supported by the CERC-CVC U.S.-China Program of Clean Vehicle under Award Number DE-PI0000012. All the calculations were performed in the PC Cluster from Sugon Company of China.

*Author to whom correspondence should be addressed: phlhj@whu.edu.cn

[1] G. A. Slack, in *CRC Handbook of Thermoelectrics*, edited by D. M. Rowe (CRC Press, Boca Raton, FL, 1995), p. 407.
[2] S. Bose, H. N. Acharya, and H. D. Banerjee, J. Mater. Sci. **28**, 5461 (1993).
[3] T. Caillat, A. Borshchevsky, and J.-P. Fleurial, J. Appl. Phys. **80**, 4442 (1996).
[4] J. Tani and H. Kido, Phys. B (Amsterdam) **364**, 218 (2005).
[5] M. Akasaka, T. Iida, A. Matsumoto, K. Yamanaka, Y. Takanashi, T. Imai, and N. Hamada, J. Appl. Phys. **104**, 013703 (2008).
[6] S. K. Bux, M. T. Yeung, E. S. Toberer, G. J. Snyder, R. B. Kanerb, and J.-P. Fleurial, J. Mater. Chem. **21**, 12259 (2011).
[7] S.-W. You and I.-H. Kim, Curr. Appl. Phys. **11**, S392 (2011).
[8] J. Tani and H. Kido, Intermetallics **15**, 1202 (2007).
[9] T. Dasgupta, C. Stiewe, R. Hassdorf, A. J. Zhou, L. Boettcher, and E. Mueller, Phys. Rev. B **83**, 235207 (2011).
[10] V. K. Zaitsev, M. I. Fedorov, E. A. Gurieva, I. S. Eremin, P. P. Konstantinov, A. Y. Samunin, and M. V. Vedernikov, Phys. Rev. B **74**, 045207 (2006).
[11] Y. Isoda, T. Nagai, H. Fujiu, Y. Imai, and Y. Shinohara, *Proceedings of the 26th International Conference on Thermoelectrics*, Jeju Island, South Korea, 2007 (unpublished).

[12]J. Tani, and H. Kido, J. Alloys Compd. **466**, 335 (2008).
[13]W. Luo, M. Yang, F. Chen, Q. Shen, H. Jiang, and L. Zhang, Mater. Sci. Eng. B **157**, 96 (2009).
[14]W. Liu, X. Tang, and J. Sharp, J. Phys. D: Appl. Phys. **43**, 085406 (2010).
[15]H. L. Gao, T. J. Zhu, X. X. Liu, L. X. Chen and X. B. Zhao, J. Mater. Chem. **21**, 5933 (2011).
[16]W. Liu, X. J. Tan, K. Yin, H. J. Liu, X. F. Tang, J. Shi, Q. J. Zhang, and C. Uher, Phys. Rev. Lett. **108**, 166601 (2012).
[17]G. Kresse and J. Hafner, Phys. Rev. B **47**, R558 (1993).
[18]G. Kresse and J. Hafner, Phys. Rev. B **49**, 14251 (1994).
[19]G. Kresse and J. Furthmuller, Comput. Mater. Sci. **6**, 15 (1996).
[20]J. P. Perdew and Y. Wang, Phys. Rev. B **45**, 13244 (1992).
[21]T. J. Scheidemantel, C. Ambrosch-Draxl, T. Thonhauser, J. V. Badding, and J. O. Sofo, Phys. Rev. B **68**, 125210 (2003).
[22]T. Thonhauser, T. J. Scheidemantel, J. O. Sofo, J. V. Badding, and G. D. Mahan, Phys. Rev. B **68**, 085201 (2003).
[23]A. Bejan and A. D. Allan, *Heat Transfer Handbook* (Wiley, New York, 2003), p. 1338.
[24][http://lammps.sandia.gov/doc/Manual.html].
[25]J. W. Che, T. Çağın, W. Q. Deng, and W. A. Goddard III, J. Chem. Phys. **113**, 6888 (2000).
[26]V. K. Zaitsev, M. I. Fedorov, I. S. Eremin, and E. A. Gurieva, *Thermoelectrics Handbook: Macro to Nano-Structured Materials* (CRC Press, New York, 2005), Chap. 29.
[27]Y. Isoda, T. Nagai, H. Fujiu, Y. Imai, and Y. Shinohara, *Proceedings of the 25th International Conference on Thermoelectrics*, Vienna, Austria, 2006 (unpublished).
[28]Y. Z. Pei, X. Y. Shi, A. LaLonde, H. Wang, L. D. Chen, and G. J. Snyder, Nature (London) **473**, 66 (2011).
[29]M. G. Holland, Phys. Rev. **132**, 2461 (1963).
[30]Q. Zhang, J. He, T. J. Zhu, S. N. Zhang, X. B. Zhao, and T. M. Tritt, Appl. Phys. Lett. **93**, 102109 (2008).
[31]M. Akasaka, T. Iida, K. Nishio, and Y. Takanashi, Thin Solid Films **515**, 8237 (2007).
[32]G. S. Nolas, D. Wang, and M. Beekman, Phys. Rev. B **76**, 235204 (2007).
[33]W. Liu, X. F. Tang, H. Li, J. Sharp, X. Y. Zhao, and C. Uher, Chem. Mater. **23**, 5256 (2011).
[34]N. Yang, G. Zhang, and B. Li, Nano Lett. **8**, 276 (2008).
[35]S. Wang, and N. Mingo, Appl. Phys. Lett. **94**, 203109 (2009).
[36]J. Zhou, X. Li, G. Chen, and R. Yang, Phys. Rev. B **82**, 115308 (2010).
[37]K. Biswas, J. He, Q. Zhang, G. Wang, C. Uher, V. P. Dravis, and M. G. Kanatzidis, Nat. Chem. **3**, 160 (2011).